EXPERIMENTAL STUDY ON PCRV-SUPPORT STRUCTURES UNDER SIMULATED EARTHQUAKE MOTION

T. SUZUKI, K. WAKAMATSU, T. TAKEDA
Ohbayashi-Gumi, Ltd., Ohbayashi-Gumi Technical Research Institute, Tokyo, Japan

T. MATSUMOTO
Ohbayashi-Gumi, Ltd., Nuclear Facility Section, Tokyo, Japan

SUMMARY

Since Prestressed Concrete Reactor Vessels (PCRV) are rigid and strong in themselves, the structural design of them may not be greatly influenced by earthquake motion. However, some restrictions resulting from piping lay-out, etc. prevent to use a support with stiffness comparable to that of the PCRV. Accordingly, the design of the support structure may give a great influence upon the response of nuclear plant system subjected to strong earthquake motion. While the intensity of earthquake motion to be considered in the design is too difficult to anticipate, it has been required to estimate the dynamic behavior of PCRV structures beyond the elastic limit.

This study is concerned with one of the experimental series for PCRV structures integral with the reinforced concrete support that appear feasible. The behaviors of the models under a static or dynamic load are compared with analytical results and discussed in this paper.

Each model used in the tests consists of a steel mass representing PCRV and a reinforced concrete hollow cylinder support. The dimension of the support is considered to be about 1/50 scale of prototype design. The models with variable heights and sectional dimensions were subjected to periodic or simulated earthquake motions at their base. For better understanding of their behaviors, static tests were performed, too.

It was pointed out from the test results that the higher the external exciting levels are, the longer natural period becomes as well as the more the damping coefficient is increased.

In the dynamic analysis, use is being made of a two-degree-of-freedom model with moment of inertia of the mass itself, and the inelastic response was calculated to be based on the proposed hysteresis taking concrete cracking and yielding of reinforcements in consideration.

From the good coincidence between tests and calculated results, it may be stated that the response of such kind of a structure beyond the elastic limit can be predicted by the dynamic analysis method used herein.

The usual assumption of larger damping value for high level of excitation may not be realistic for the prediction of dynamic response of the reinforced concrete structures. Because once cracking of concrete is initiated, drastic changes in the periodicity of the structures may be observed which will cause larger displacements.—Due attention has to be paid to this point in the aseismic design of PCRV structures.

I. Introduction

The PCRV being rigid and strong in themselves, the structural design of them may not be greatly influenced by earthquake motion. However, some restrictions resulting from piping lay-out, etc. prevent the use of supports with stiffness comparable to that of PCRV. Accordingly, the design of support structure may give a great influence upon the response of nuclear power plant system subjected to strong earthquake motion. While the intensity of earthquake motion to be considered in the design is too difficult to anticipate, it has been required to estimate the dynamic behavior of PCRV structure beyond elastic limit considering varying stiffness and energy absorption after initiations of concrete cracks and yielding of reinforcement of PCRV support.

II. Experimental Study

II-1 Test Specimen

General description of test specimen and dimension of 6 specimens are given in Fig. 1 and Table 1. General arrangement of reinforcement are given in Fig. 2. Construction joint was made at a-a' section to allow removal of the form.

Yielding strength and Young's modulus of reinforcement were σ_y = 3800 kg/cm^2 and Es = 1.9 x 10^6 kg/cm^2 respectively. Compressive test results of the concrete tested just prior to the experiment are given in Table 1.

II-2 Static Load Test

II-2-1 Test Procedure

Two models (No. 12-1, No. 22-1) were fixed on the test floor with 4 anchor bolts and lateral load was alternately applied at the centroid of the steel mass with oil jack to study the elastic rigidity, initial crack load, yield load and deflection, and load-deflection relationships.

Deflections and strains were measured with dial-gage and strain gages, respectively.

II-2-2 Test Results

Load-Deflection Relation

Fig. 3 and 4 show the load-deflection relationships at the centroid of the steel mass of Models 12-1 and 22-1, respectively. These two hysteresis curves show rather small energy absorption characteristic to the load reversals below the yield level. With Model 22-1, the ultimate load reached was 10.5 ton, owing to the crushing of concrete at the compression side. With Model 12-1, the test was not carried out to the ultimate condition.

Crack and Yield

Loads at the bending crack, shear crack and yield are given in Table 2. The state of cracks after tests of Model 12-1 are shown in Fig. 5. The numbers written beside the crack lines in the figure indicate the lateral load at the occurrence of that

particular crack. The crack pattern of positive loading is similar to that of negative loading.

II-2-3 Analysis

Linear Analysis

The elasticity was calculated by two methods. Finite Element Method and Beam Theory in which the deformations of slabs above and below the support were taken into account. There wasn't much difference between these two calculated values.

Non-Linear Analysis

a) Crack Load

Crack initiation load Qc was calculated with following formula:

$$Qc = (2\sqrt{Fc} + N/A)\ Z$$

where Fc = compressive strength of concrete at the test stage (kg/cm^2)

N = axial load (kg)

A = sectional area (cm^2)

Z = section modulus (cm^3)

b) Yield Load and Yield Deflection

The yield load Qy for bending moment was calculated on the basis of the following three assumptions.

(1) strain in the reinforcing bar and concrete is directly proportional to the distance from the neutral axis.

(2) stress-strain relationship of concrete is elastic for compression side and tensible strength is zero.

(3) Qy is the load when the outermost reinforcement yields in tension.

The yield deflection Dy was assumed to be the sum of the following three parts.

(1) bending deflection based on crack section.

(2) deflection caused by slip of the reinforcement and it was simply assumed that both curvatures, at the top and bottom of cylinder support, were extended into slabs for length equal to 10 times the bar diameter.

(3) elastic deflection caused by shear.

With Model 12-1, for example, the relative contribution of the three parts to the total deflection were as follows:

part 1	68.7%
part 2	28.9%
part 3	2.4%

II-2-4 Comparison between the Test and the Calculated Results

The primary curves of two models calculated analytically are shown in Figs. 3 and 4 as three linear segment lines. Table 3 gives the test and the calculated results of Models 12-1 and 22-1. Test results here are the average values of positive and negative

loads. They are in very good coincidence with each models.

II-3 Vibration Test

II-3-1 Earthquake Simulator

Earthquake Simulator at Ohbayashi-Gumi's Technical Institute is electro-hydraulic type (Fig. 6), performance curves of earthquake simulator are given in Fig. 7.

II-3-2 Test Procedure

Experiment was conducted to study the transformation of dynamic characteristic within the elastroplasticity area. Test specimen was fixed on the vibration test floor as shown in Fig. 8 for high input sine wave or Eℓ-Centro (1940 N-S) seismic wave to be input (H·R) toward progressing destruction. Then free vibration (F·V) and low level input steady vibration (S·S) was conducted to study transformation of dynamic characteristic. Therefore H·R, F·V, and S·S form the serial for vibration test cycle. Test specimen 12-2, 22-2 and 21 were gradually destroyed under base motions of sine wave only by changing input cycle and input acceleration. Input frequency etc. were determined to increase response displacement based upon natural frequency obtained in the previous test.

For high input tests (H·R), 20 to 30 sine waves were input whereas simulated earthquake motion (EL-Centro N-S 1940) was generated such that 30 seconds of original record was compressed into 15 seconds.

Model 12-2 test procedure is given in Table 4 as an example. Response values listed therein were values at the centroid of the mass.

II-3-3 Test Results

(1) Resonance Curve

Resonance curves of the specimens (Models 12-2, 22-2, 13 and 21) obtained from the steady state experiments (S·S) are given in Fig. 9. Two numerals appearing above each peak, in these figures, are the values of response acceleration at the top and the centroid of the mass respectively.

(2) Appraisal of Rotational Spring

Rotational spring (K_R) is calculated from the relation between moment and rotational angle obtained from experimental record;

$$K_R = 3.08 \times 10^6 \text{ ton·cm}$$

The measured and calculated values of the 1st natural frequency are also given in Table 5. Calculated values are the case with rocking spring at the base. Experimental values agree well with the calculated results.

(3) Mode

The first mode of resonance obtained from experiment and

calculated are shown together in Fig. 10.

(4) Variation of stiffness and Damping

The variation of stiffness and damping obtained from the resonance curves and free vibrations after large input (Test H·R) and the equivalent stiffness* are shown in Fig. 11.

* equivalent stiffness (K eq. t/cm) is calculated in each test (H·R) as follows.

$$K\ eq = \frac{Q}{Dmax}$$

where Dmax = measured maximum displacement at the centroid of steel mass

Q = lateral force calculated by multiplying mass by measured maximum acceleration at the centroid

In these figures, the calculated equivalent stiffness considering the effect of rotational spring at the base are shown by solid lines. What is evident from these figures is that the stiffness decrease profoundly from crack stage to yield stage and after yield, both equivalent stiffness and stiffness obtained from resonance curve has a tendency of following along the calculated equivalent stiffness line. However the stiffness in small input level is rather hard in comparison with the stiffness in large input level.

The damping coefficient has a tendency to increase from about 2% to almost 6% as the experienced maximum displacement increase.

III. Dynamic Experiment Analysis

III-1 Analysis

Simple lumped-mass model considering 2 variables, rotation angle (θ) and lateral displacement (y), was used as an analytical model as shown in Fig. 12.

From Fig. 12, displacement Z at the centroid of mass is

$$Z = x + y + e\theta \qquad (1)$$

where x = lateral displacement at the base

y = lateral displacement at the top of the support to the base

θ = rotation angle of mass

e = distance from the top of cylindrical support to the centroid of mass including the effect of top slab

Then load-deflection relationship at the top of cylindrical support is expressed as follows:

$$y = \alpha_{11}P + \alpha_{12}M \qquad \theta = \alpha_{21}P + \alpha_{22}M \qquad (2)$$

where P = laterail force, M = moment,

α = influence coefficient

Eq.(2) expressed in dynamic balance formula (ignore the mass of support)

$$-y = \alpha_{11} m(\ddot{x} + \ddot{y} + e\ddot{\theta}) + \alpha_{12}\left\{ me(\ddot{x} + \ddot{y} + e\ddot{\theta}) + J\ddot{\theta} \right\}$$
$$-\theta = \alpha_{21} m(\ddot{x} + \ddot{y} + e\ddot{\theta}) + \alpha_{22}\left\{ me(\ddot{x} + \ddot{y} + e\ddot{\theta}) + J\ddot{\theta} \right\} \quad (3)$$

where m = total mass of steel and top slab

J = rotatory inertia of mass about its centroid

Eq.(3) in matrix expression

$$\begin{bmatrix} \alpha_{11} & \alpha_{12} \\ \alpha_{21} & \alpha_{22} \end{bmatrix} \begin{bmatrix} m & me \\ me & me^2+J \end{bmatrix} + \begin{Bmatrix} y \\ \theta \end{Bmatrix} = -\ddot{x} \begin{bmatrix} \alpha_{11} & \alpha_{12} \\ \alpha_{21} & \alpha_{22} \end{bmatrix} \begin{Bmatrix} m \\ me \end{Bmatrix} \quad (4)$$

Multiply Eq.(4) by $|\alpha|^{-1}$ and internal viscous damping is assumed.

$$\begin{bmatrix} m & me \\ me & me^2+J \end{bmatrix} \begin{Bmatrix} \ddot{y} \\ \ddot{\theta} \end{Bmatrix} + \begin{bmatrix} C_{11} & C_{12} \\ C_{21} & C_{22} \end{bmatrix} \begin{Bmatrix} \dot{y} \\ \dot{\theta} \end{Bmatrix} + \begin{bmatrix} K_{11} & K_{12} \\ K_{21} & K_{22} \end{bmatrix} \begin{Bmatrix} y \\ \theta \end{Bmatrix} = - \begin{Bmatrix} m \\ me \end{Bmatrix} \ddot{x} \quad (5)$$

where $[K]$ = stiffness matrix

$[C] = \beta [K]$ damping matrix

β = coefficient

With non-linear response analysis, step by step analysis was made on following assumption:

1. Stiffness matrix in Eq.(5) was changed on the basis of stiffness reduction as to the lateral deflection at the centroid of mass.
2. As for the load-deflection hysteresis, the stiffness reduction was based on the primary curve beforementioned for monotonus increasing load. When unloaded, as given in Fig. 13, after initiations of concrete cracks or yielding of reinforcement, the stiffness was degraded by amount of the ratio of elastic rigidity (C) to trangential stiffness (C_1) or (C_2).
3. In damping matrix $[C] = \beta [K]$, $[K]$ was kept constant and coefficient β was only varied to take following percentage of critical damping;

elasticity	0.02%
from crack to yield	0.04%
after yield	0.06%

III-2 Comparison between the Test Results and the Calculated Results

With Model 21 and 13 comparison is to be made of measured response and calculated response at the centroid of mass based upon aforementioned assumptions. Test in which reinforcement did not yield after cracking at support is to be called RUN-1, whereas Test in which reinforcement yield is to be called RUN-2 hereafter.

Model 21

Input base motions were sinusoidal. Measured and calculated responses are given in Fig. 14. Input frequency, maximum accelerations and maximum values of measured and calculated response are given in Table 6. Measured maximum deflections in RUN-1 and in RUN-2 are about 0.84 times and about 2.5 times as much as the yield deflection, respectively. According to the measured responses, both in RUN-1 and

in RUN-2, the maximum acceleration and deflection were reached immediately after tests started, although the intensity of the base motions were rather small. Because the input frequency was chosen to be very close to the natural period of the model in each run, the model was in resonance. After that, however, the response values got rather smaller. This is because of drastic change in stiffness due to the crack initiation of concrete or yielding of reinforcement. These tendency were observed in the calculated response too.

Model 13

Input base motions EL-Centro 1940 N-S modified as mentioned before was used. Measured and calculated non-linear responses are given in Fig. 15. Similarly, maximum input acceleration and maximum values of responses are compiled in Table 7. Measured maximum deflections in RUN-1 and RUN-2 are about 0.33 and 1.3 times as much as yield deflection respectively. The prediction of response is satisfactory.

Elastic response spectrum of Model 13 at RUN-1 and RUN-2 are given in Fig. 16, where the maximum base accelerations are increased to 980 gal. Table 8 gives the maximum response values of elastic system with 2% critical damping to RUN-1 and RUN-2.

Compared Table 7 with Table 8, calculated elastic response, both acceleration and displacement are approximately same values as measured ones in RUN-1 which performed a stress level in the crack initiation. However, with RUN-2 where yielding of reinforcement took place, when linear responses is compared with measured results, acceleration response is 2.7 times larger whereas displacement response is nearly equal. In linear response analysis, if response acceleration to be equal to the measured one by using larger damping, the response displacement is to be smaller than measured one.

Conclusion

1. From static load test results, it may be said that the load and deflection at the time of concrete cracking and reinforcement yielding which constitute primary curve can be theoretically predicted.
2. Elastic period obtained at vibration test closely resembled to theoretical value, whereas, percentage of critical damping obtained was approximately 2%.
3. With the vibration test, following appearance of cracks, change in rigidity and energy absorption capacity was notable, and in comparison with elastic response period has become longer and displacement response become greater whereas acceleration become smaller.

   It is believed that care must be exercised in determining the deformation limit in the designing process of piping works for the machinery.
4. With use of proposed simple hysterical model based on the primary curve and with adequately assumed damping, the non-linear response of reinforced concrete structure to strong earthquake motion may be predicted.

Table 1 Dimension of the supports

Model Number	12-1 12-2	13	21	22-1 22-2
Height (cm)	30	15	60	30
Wall thickness (cm)	4	4	4	4
Outer diameter (cm)	40	40	60	60
Initial axial stress (㎏/)	24.04	24.04	15.45	15.45
Reinforcement ratio (AS/AC) (%)	1.273	1.273	0.820	0.820
Compressive strength (㎏/)	291. 292.	318.	360.	331. 289.
Young's modulus (×10⁵㎏/)	2.22 2.36	2.25	2.17	2.27 2.38

Table 4 Test procedure

Test No.	Remarks (I)	Remarks (II)
F-V - 0	after set over	
S-S - 0	after set over	
H-R - 1	Input; Freq. 7.8Hz Acc. 60 gal Resp.; Disp. 1mm Acc. 150 gal	Bend crack at the lower part
F-V - 1	after H R-1	
S-S - 1	after H R-1	
H-R - 2	Input; Freq. 4.7Hz Acc. 300 gal Resp.; Disp. 4.5 mm Acc. 400 gal	Bend crack at the upper part field
F-V - 2	after H R-2	
S-S - 2	after H R-2	
H-R - 3	Input; Freq. 4 Hz Acc. 150 gal Resp.; Disp. 9 mm Acc. 300 gal	Shear crack
F-V - 3	after H R-3	
S-S - 3	after H R-3	

Table 2 Static test results

Model	Load direction	Bend crack	Shear crack	Yield
12 - 1	Positive	2.8 ton	3.6 ton	4.2 ton
	Negative	2.2	3.4	4.0
22 - 1	Positive	4.5	5.5	7.0
	Negative	4.0	5.5	6.5

Table 3 Comparison between the test and the calculated results

		Elastic rigidity	Bend crack load	Shear crack load	Yield load	Yield deflection
12-1	Test	47.8 t/cm	2.50 ton	3.50 ton	4.10 ton	2.50 mm
	Calculated	47.2	2.18		4.13	2.43
22-1	Test	156.0	4.25	5.50	6.75	1.78
	Calculated	177.0	4.04		6.65	1.39

Table 6 Measured and calculated responses (Model 21)

	Base Acceleration (Frequency)	Response Acceleration		Response Displacement	
		Experiment	Calculation	Experiment	Calculation
RUN - 1	112 gal (7.0 Hz)	480 gal	462 gal	2.55 mm	2.60 mm
RUN - 2	205 gal (4.7 Hz)	505 gal	520 gal	7.60 mm	7.73 mm

Table 7 Measured and calculated responses (Model 13)

	Base Acceleration	Response Acceleration		Response Displacement	
		Experiment	Calculation	Experiment	Calculation
RUN - 1	180 gal	240 gal	235 gal	0.59 mm	0.58 mm
RUN - 2	410 gal	470 gal	500 gal	2.40 mm	2.50 mm

Table 5 1st natural frequency

MODEL	Experiment	Calculation
12 - 2	8.9 Hz	8.9 Hz
22 - 2	13.5	13.4
13	11.2	12.0
21	8.6	9.3

Table 8 Linear responses

	Acceleration	Displacement
RUN - 1	270 gal	0.61 mm
RUN - 2	1330 gal	2.64 mm

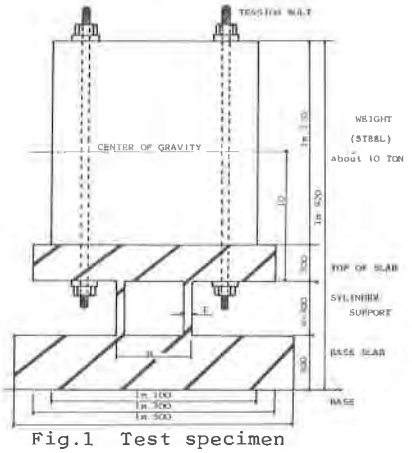

Fig.1 Test specimen

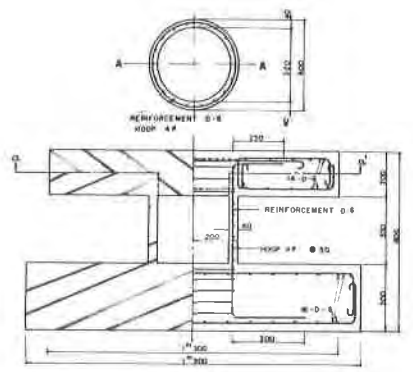

Fig.2 Arrangement of reinforcement

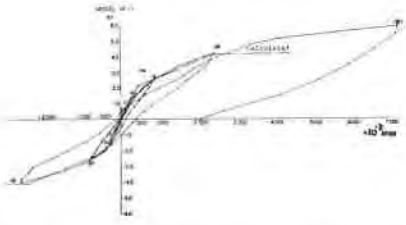

Fig.3 Load-deflection curve

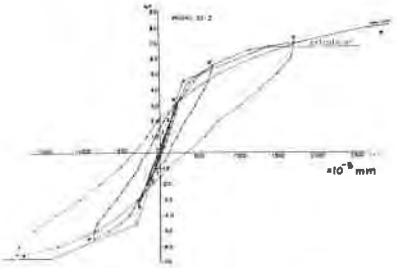

Fig.4 Load-deflection curve

The direction of application of load

The direction perpendicular to the plane of action of load

Fig.5 Crack initiation

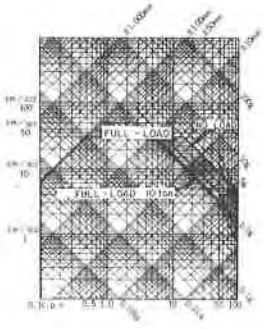

Fig.7 Performance curves of earthquake simulator

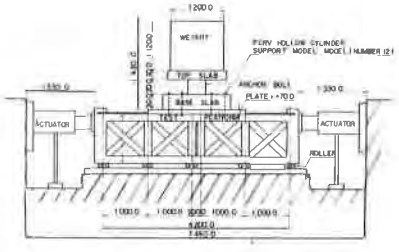

Fig.6 Earthquake simulator

Fig.8 Vibration test

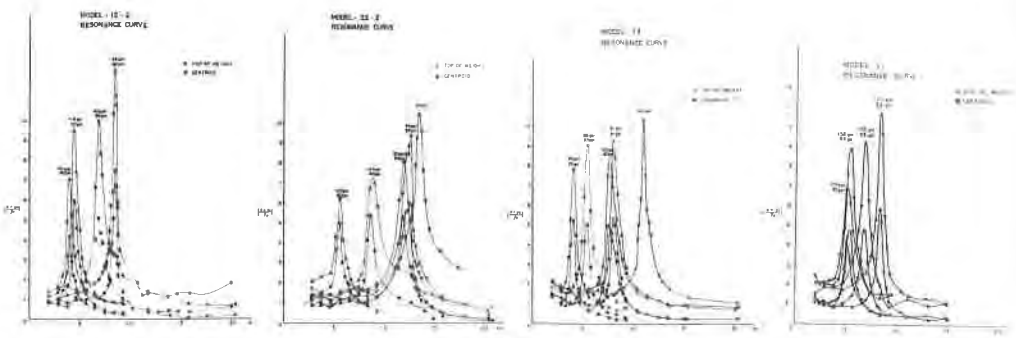

Fig. 9 Resonance curves

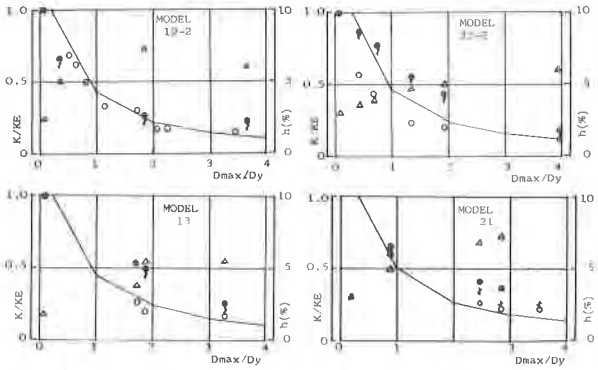

: stiffness result from H·R test
: stiffness result from resonance
: stiffness result from free vibration
: damping ratio

Fig.11 Variation of stiffness and damping

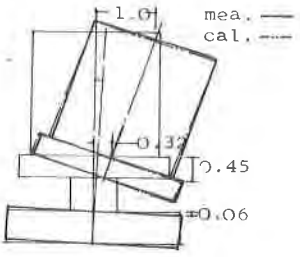

Fig.10 1st Mode

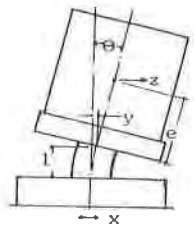

Fig.12 Analytical model

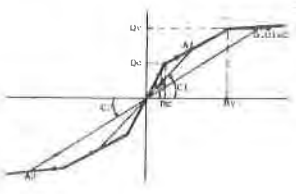

Fig.13 Assumed hysteresis

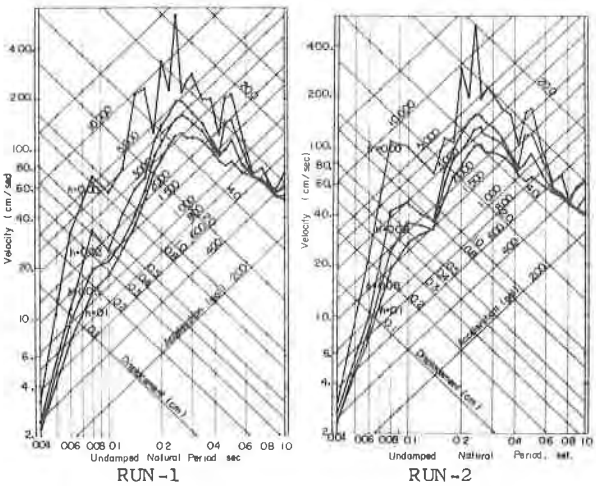

Fig.16 Response spectrum

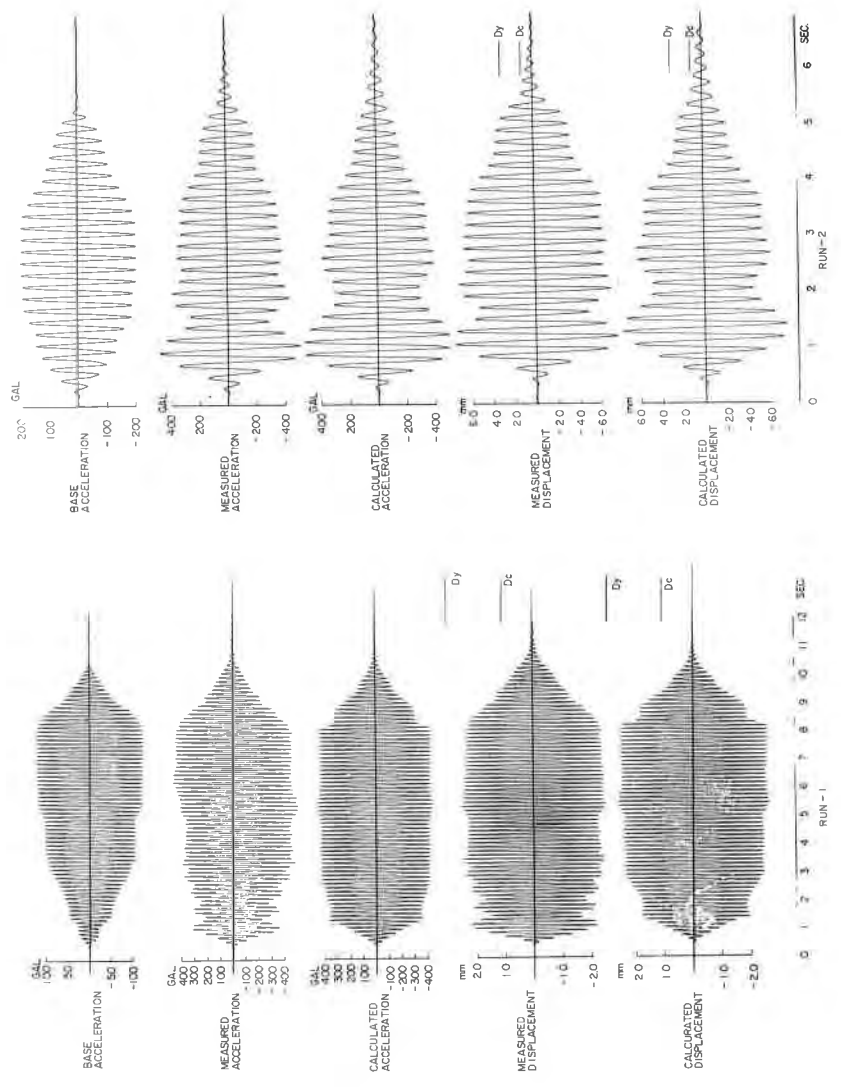

Fig.14 Measured and calculated responses (Model 21)

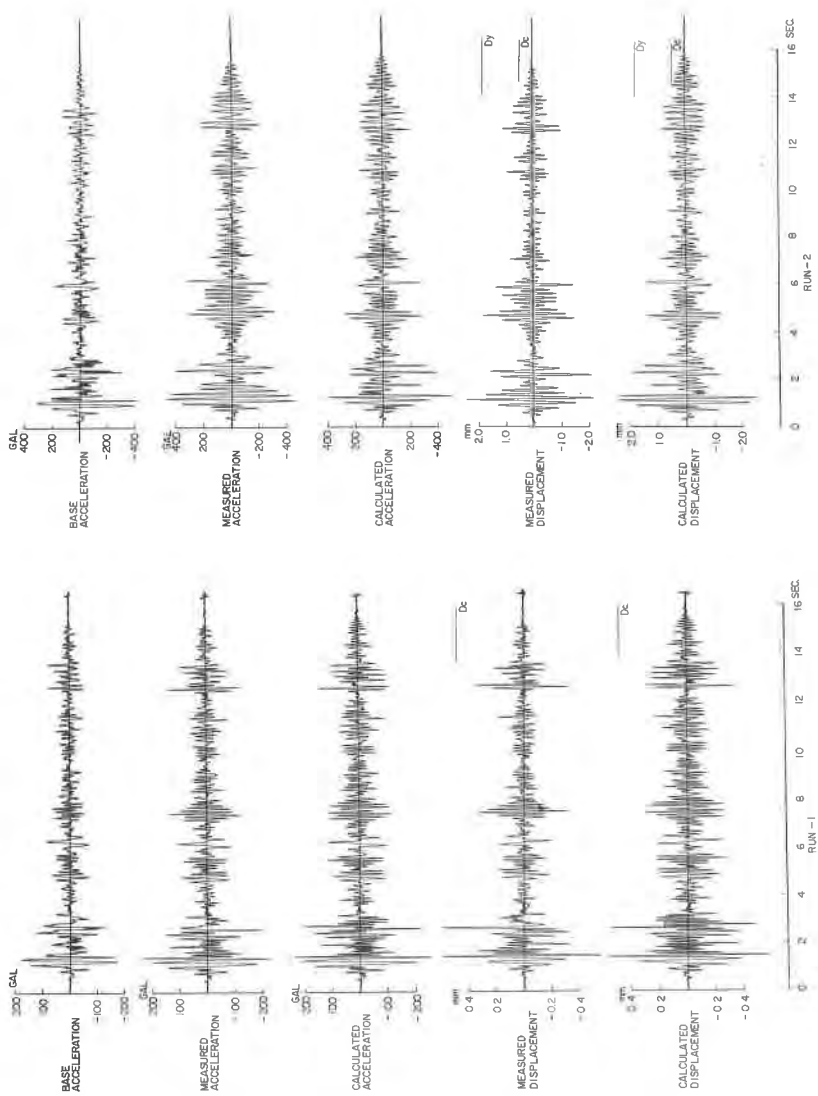

Fig. 15 Measured and calculated responses (Model 13)